19. A. S. de Groot *et al.*, *AIDS Res. Hum. Retroviruses* **13**, 529 (1997).
20. N. V. Sipsas *et al.*, *J. Clin. Invest.* **99**, 752 (1997).
21. L. Wagner *et al.*, *Nature* **391**, 908 (1998).
22. P. O. Campos-Lima *et al.*, *Science* **260**, 98 (1993).
23. P. O. Campos-Lima, V. Levitsky, M. P. Imreh, R. Gavioli, M. G. Masucci, *J. Exp. Med.* **186**, 83 (1997).
24. C. M. Hay *et al.*, *J. Virol.* **73**, 5509 (1999).
25. C. Brander *et al.*, *J. Clin. Invest.* **101**, 2559 (1998).
26. P. Shankar, H. Sprang, J. Lieberman, *J. AIDS Hum. Retrovirol.* **19**, 111 (1998).
27. S. Rowland-Jones *et al.*, *Nature Med.* **1**, 59 (1995).
28. K. R. Fowke *et al.*, *Lancet* **348**, 1347 (1996).
29. S. L. Rowland-Jones *et al.*, *J. Clin. Invest.* **102**, 1758 (1998).
30. S. L. Rowland-Jones *et al.*, *Immunol. Lett.* **66**, 9 (1999).
31. S. Mazzoli *et al.*, *Nature Med.* **3**, 1250 (1997).
32. G. Fabio *et al.*, *Clin. Exp. Immunol.* **87**, 20 (1992).
33. The viral load assay used until November 1999 was the HIV Amplicor (Roche Diagnostics, Branchburg, NJ) (lower limit of detection, 400 copies per ml). The Roche Amplicor HIV monitor version 1.5, Ultrasensitive (lower limit of detection, 50 copies per ml) was used thereafter.
34. P. J. R. Goulder *et al.*, *Immunol. Rev.* **159**, 17 (1997).
35. M. Schmitt *et al.*, *AIDS* **14**, 653 (2000).

36. We are indebted to participants in the WA HIV Cohort Study as well as past and present clinical and laboratory staff of the Department of Clinical Immunology and Biochemical Genetics, Royal Perth Hospital, Western Australia. We thank S. Rowland-Jones for helpful comments on the manuscript. C.B.M. was recipient of an Australian Postgraduate Award, and M.J. is recipient of a National Health and Medical Research Council of Australia Postgraduate Scholarship.

9 January 2002; accepted 27 March 2002

Magneto-Opto-Electronic Bistability in a Phenalenyl-Based Neutral Radical

M. E. Itkis, X. Chi, A. W. Cordes, R. C. Haddon*

A new organic molecular conductor, based on a spiro-biphenalenyl neutral radical, simultaneously exhibits bistability in three physical channels: electrical, optical, and magnetic. In the paramagnetic state, the unpaired electrons are located in the exterior phenalenyl units of the dimer, whereas in the diamagnetic state the electrons migrate to the interior phenalenyl units and spin pair as a π-dimer. Against all expectations, the conductivity increases by two orders of magnitude in the diamagnetic state, and the band gap decreases. This type of multifunctional material has the potential to be used as the basis for new types of electronic devices, where multiple physical channels are used for writing, reading, and transferring information.

The processing of information is based on the ability to control and retrieve changes in a particular physical property of a material, such as the electrical, magnetic, or optical response. Usually, at the level of the basic unit, one of these physical channels is used. When two different physical channels of the material are simultaneously involved, a new breadth of applications and even new fields of research often appear, such as optoelectronics, magnetooptics, and spintronics (*1*), which, as Das Sarma (*2*) noted, "is a seamless integration of electronic, optoelectronic and magnetoelectronic multifunctionality on a single device. . . ." We now report that a phenalenyl-based neutral radical organic conductor exhibits bistability just above room temperature so that one state is paramagnetic, insulating, and infrared (IR) transparent. These properties reverse in the other state to produce a material that is diamagnetic, conducting, and IR opaque.

By definition, neutral organic radical molecules contain an unpaired electron just as in a classical (mono)atomic metal, and they are promising basic units for the construction of an intrinsic molecular metal or superconductor (*3*). The basic molecular building block on which we report consists of two phenalenyl ring systems, spiro-conjugated through a boron atom (Fig. 1), so that the two halves of the molecule are orthogonal to one another. This nonplanar unit prevents the formation of a one-dimensional structural chain (*4*, *5*), thus obviating the occurrence of a Peierls transition to an insulating ground state (*6*).

A variety of alkyl (C_nH_{2n+1}) groups can be attached to the nitrogen atoms to modify the crystal packing; the first phenalenyl-based neutral radical to be crystallized [**1**, with a hexyl group ($n = 6$) attached to nitrogen] is a resonance-stabilized carbon-based free radical (*7*). The existence of the monomeric, neutral carbon-based free radical **1** in the crystalline state is unprecedented; all prior structures have required steric hindrance to inhibit dimerization (*4*, *5*, *8*, *9*). Furthermore, the hexyl radical **1** shows the highest conductivity of any neutral organic molecular solid, despite the fact that all intermolecular contacts are outside of the van der Waals spacing (*7*).

Changing the alkyl group from hexyl **1** to butyl **2** or ethyl **3** leads to a crystal structure containing π-dimers as the basic building block (Fig. 1) (*10*). In the high-temperature limit [**3**, temperature (T) > 350 K], the interplanar distance within the π-dimer is about 3.3 Å and the interaction is sufficiently weak that the electron spins remain unpaired. The dimerization to a diamagnetic state occurs at a structural phase transition when T decreases below 320 K and

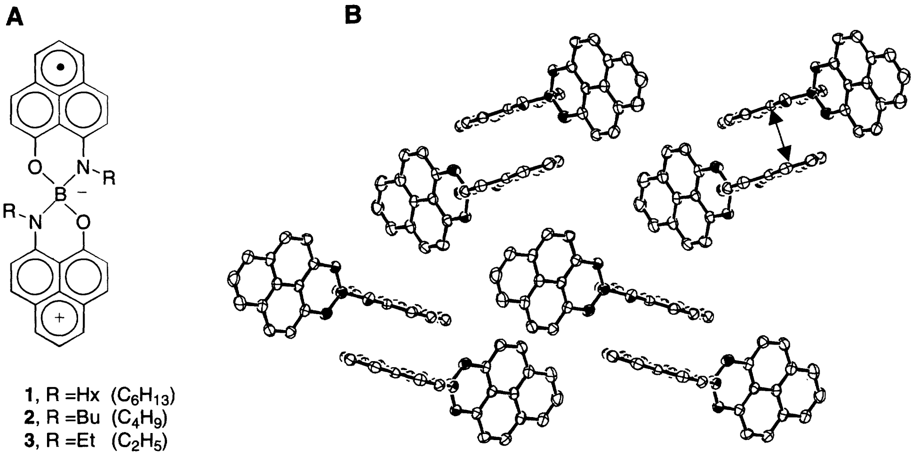

Fig. 1. (**A**) Molecular structure of neutral radicals. (**B**) X-ray crystal structure of ethyl radical **3**, showing the intra-dimer distance, *d*, indicated by the double-headed arrow. *d* increases from ~3.2 to ~3.3 Å as the spins unpair and the compound becomes paramagnetic.

Center for Nanoscale Science and Engineering, Departments of Chemistry and Chemical & Environmental Engineering, University of California, Riverside, CA 92521–0403, USA.

*To whom correspondence should be addressed. E-mail: haddon@ucr.edu

the intradimer distance contracts to about 3.2 Å. In low-dimensional systems, dimerization results in an energy gap at the Fermi level and leads to an insulating ground state (*6*).

The transmittance spectra of a single crystal of **3** above and below the phase transition (Fig. 2A) shows that, in contrast with expectations based on the Peierls theorem, the optical gap actually closes on dimerization. A similar effect also occurs with **2** (Fig. 2B), but in this case the transition temperature is changed drastically, from 335 to 135 K. The hexyl radical **1** does not undergo a structural phase transition (*7*) and remains momomeric over the entire temperature range; the change in the energy gap is minimal between 1.8 and 300 K (Fig. 2C). Note that increasing the length of the alkyl chain leads to an increase in the cut-off frequency of the transmission spectra (ω_c), which is related to the energy gap: $\omega_c = 2900\ \mathrm{cm}^{-1}$ for $n = 2$ (**3**) (Fig. 2B), $\omega_c = 3500\ \mathrm{cm}^{-1}$ for $n = 4$ (**2**) (Fig. 2A), and $\omega_c = 4300\ \mathrm{cm}^{-1}$ for $n = 6$ (**1**) (Fig. 2C).

The bistability in optical, electrical, and magnetic properties of the butyl radical **3** is shown in Fig. 3. The changes in all three physical channels occur as a first-order phase transition with a hysteretic loop 25-K wide, centered around 335 K. The IR transmittance changes from being optically transparent in the high-temperature limit to being opaque in the diamagnetic state. The hysteresis loop corresponds to IR radiation at wavelength (λ) = 3.85 μm (2600 cm^{-1}), although the bistability also appears at a variety of IR bands between 3 and 11 μm (3300 to 900 cm^{-1}) (Fig. 2A), matching a number of IR lasers and the atmospheric window in the vicinity of λ = 10 μm.

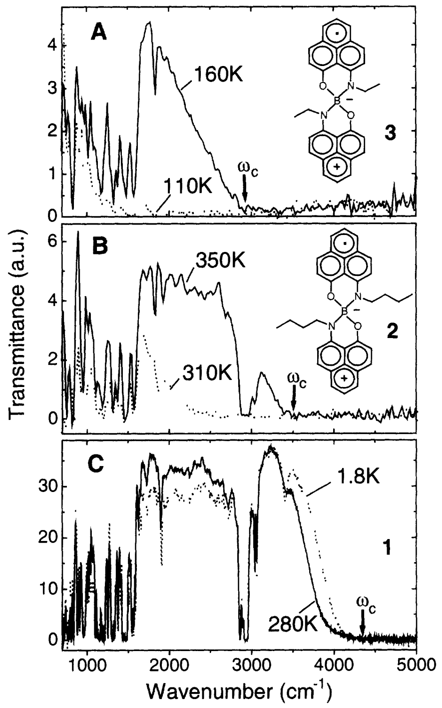

Fig. 2. IR transmittance of single crystals of spiro-biphenalenyl neutral radicals. (**A**) ethyl radical **3**; (**B**) butyl radical **2**; (**C**) hexyl radical **1**. (A) to (C) show the high-temperature (paramagnetic π-dimer) state (represented by the solid lines) and the low-temperature (diamagnetic π-dimer) state (represented by the dotted lines). The arrows indicate cut-off frequencies of the transmittance (ω_c).

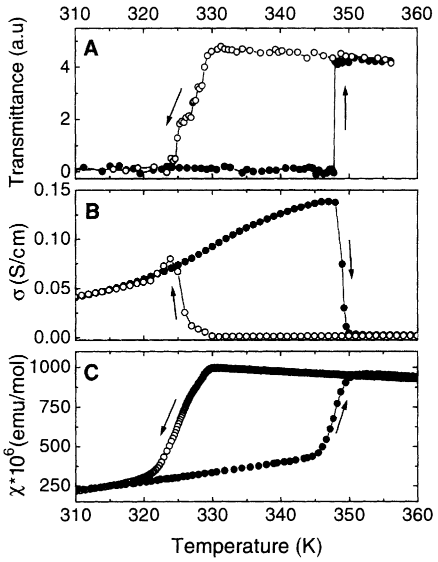

Fig. 3. Bistability in (**A**) IR transmittance at 3.85 μm, (**B**) conductivity (σ), and (**C**) magnetic susceptibility (χ), arising from the hysteretic phase transition in butyl radical **2**. The open circles represent the cooling part of the temperature cycle, and the closed circles represent the heating part. The arrows indicate the direction of the temperature sweep.

The electrical properties of the butyl radical crystal switch from an insulating to a conducting state as a result of the dimerization (Fig. 3B). The conductivity increases by two orders of magnitude at the phase transition. Although the transition to a conducting state is an unusual result for a dimerization process, it correlates with the closure of the energy gap (Fig. 2A), if the electron (hole) transport involves thermal activation of the carriers across the IR energy gap.

The high-temperature state shows a paramagnetic Curie temperature dependence of the magnetic susceptibility (χ), with one independent spin per molecule (Fig. 3C). At the phase transition, χ decreases sharply and the paramagnetism is almost completely quenched. Thus, the butyl radical **3** demonstrates a well-defined bistability in its optical, magnetic, and conducting properties, and the bistability window of 325 to 350 K is in the vicinity of room temperature, which is important for potential applications (*11*).

The bistability observed in the butyl radical is a result of a structural phase transition, but the dimerized state does not behave as a Peierls insulator. It is of interest to understand the origin of the bistabililty in these radicals and the nature of the process that drives the dimerization. Figure 4 shows our model of a π-dimer—the key structural unit in the crystal lattice that is responsible for the bistability. A bond-length analysis conducted on the basis of x-ray measurements (*7*, *10*) shows that, in the high-temperature state, the unpaired electron resides mainly on the phenalenyl units not directly involved in the π-dimer (Fig. 4), in agreement with the magnetic data that show Curie paramagnetism with one spin per molecule (Fig. 3C). At the phase transition, the unpaired electrons switch positions to the phenalenyl units that are directly involved in the π-dimer and couple to form a diamagnetic state (Fig. 4, bottom). Thus, intramolecular electron switching controls the transition of the butyl radical crystal from a high-spin, low-conductivity, IR-transparent state to a low-spin, high-conductivity, opaque state.

Magnetic bistability, with a hysteresis loop at room temperature, has been reported in molecular systems, such as doped spin-crossover compounds (*11*, *12*), and in the 1,3,5-trithia-2,4,6-triazapentalenyl organic radical (*13*). In some cases, the magnetic transition is accompanied by a change of color (*11–13*). Light-induced switching of the spin state was also reported for molecular magnetic systems, but only at cryogenic temperatures (*14*). In

Fig. 4. Interconversion between the diamagnetic π-dimer (low-temperature form) and the paramagnetic π-dimer (high-temperature form) of ethyl radical **3**.

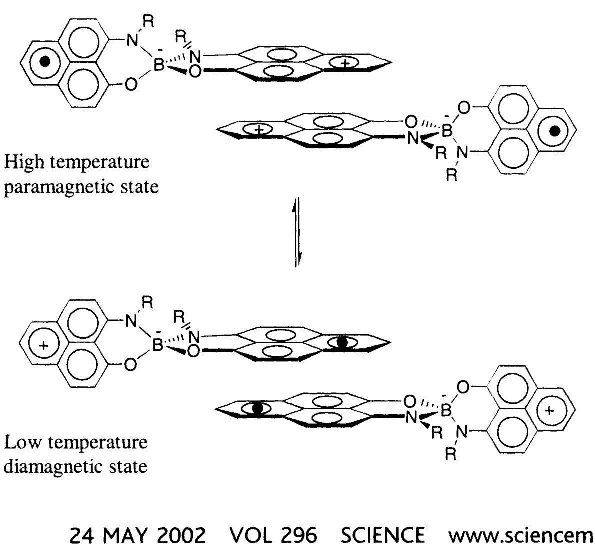

these examples, one or two different physical channels work together; in the present work, we report an organic crystal that simultaneously exhibits bistability in three physical channels: optical, electrical, and magnetic. Moreover, the basic molecular building block can be varied to change the bistability temperature range and the energy gap (which controls the optical and electrical properties).

References and Notes

1. S. A. Wolf *et al.*, *Science* **294**, 1488 (2001).
2. S. Das Sarma, *Am. Sci.* **89**, 516 (2001).
3. R. C. Haddon, *Nature* **256**, 394 (1975).
4. H. Sitzmann *et al.*, *J. Am. Chem. Soc.* **115**, 12003 (1993).
5. P. A. Koutentis *et al.*, *J. Am. Chem. Soc.* **123**, 3864 (2001).
6. R. E. Peierls, *Quantum Theory of Solids* (Clarendon Press, Oxford, 1955).
7. X. Chi *et al.*, *J. Am. Chem. Soc.* **121**, 10395 (1999).
8. M. Ballester, *Acc. Chem. Res.* **18**, 380 (1985).
9. K. Goto *et al.*, *J. Am. Chem. Soc.* **121**, 1619 (1999).
10. X. Chi *et al.*, *J. Am. Chem. Soc.* **123**, 4041 (2001).
11. J. Krober, E. Codjovi, O. Kahn, F. Groliere, C. Jay, *J. Am. Chem. Soc.* **115**, 9810 (1993).
12. O. Kahn, C. J. Martinez, *Science* **279**, 44 (1998).
13. W. Fujita, K. Awaga, *Science* **286**, 261 (1999).
14. K. Nakatani, P. Yu, *Adv. Mater.* **13**, 1411 (2001).
15. Supported by the Office of Basic Energy Sciences, Department of Energy, under grant number DE-FG03-01ER45879.

28 February 2002; accepted 10 April 2002

Binary Asteroids in the Near-Earth Object Population

J. L. Margot,[1]* M. C. Nolan,[2] L. A. M. Benner,[3] S. J. Ostro,[3] R. F. Jurgens,[3] J. D. Giorgini,[3] M. A. Slade,[3] D. B. Campbell[4]

Radar images of near-Earth asteroid 2000 DP107 show that it is composed of an ~800-meter-diameter primary and an ~300-meter-diameter secondary revolving around their common center of mass. The orbital period of 1.755 ± 0.007 days and semimajor axis of 2620 ± 160 meters constrain the total mass of the system to $4.6 \pm 0.5 \times 10^{11}$ kilograms and the bulk density of the primary to 1.7 ± 1.1 grams per cubic centimeter. This system and other binary near-Earth asteroids have spheroidal primaries spinning near the breakup point for strengthless bodies, suggesting that the binaries formed by spin-up and fission, probably as a result of tidal disruption during close planetary encounters. About 16% of near-Earth asteroids larger than 200 meters in diameter may be binary systems.

A small number of asteroids in the main belt between Mars and Jupiter have been shown to have satellites (*1–4*). The presence of a satellite, large or small, allows direct measurements of asteroid masses, which in turn place strong constraints on their density, composition, and internal structure. It raises questions about formation and dynamical evolution and has important implications for our understanding of collisional and disruption processes in the solar system. Speculations about the existence of binary asteroids in the near-Earth population, a dynamically and collisionally distinct class of objects with orbits crossing those of the inner planets, have been made on the basis of the terrestrial impact cratering record, which shows a number of crater pairs (*5*), and on the basis of anomalous lightcurve observations, which show signatures indicative of occultations or eclipses (*6*). Because the lightcurve variations can be due to shape, albedo, spin state, or a combination of those factors, the interpretation of those data sets in terms of binary asteroids has not been universally accepted.

Radar observations provide unambiguous detections of binary asteroids because images at decameter resolution can resolve the individual components. Our observations with the Arecibo and Goldstone radar systems revealed the binary nature of asteroid 2000 DP107 (*7*, *8*), which we describe in this paper, and subsequently of asteroids 2000 UG11, 1999 KW4, 1998 ST27, and 2002 BM26 (*9–12*). Asteroid 2000 DP107 was discovered by MIT Lincoln Laboratory's near-Earth asteroid search program (*13*) (LINEAR) on 29 February 2000 at a geocentric distance of 0.6 astronomical units (AU). Its orbit (semimajor axis a = 1.37 AU, eccentricity e = 0.38, inclination i = 8.7°) brought the asteroid within 0.048 AU of Earth, about 19 lunar distances, on 19 September 2000.

Doppler spectra obtained with the 3.5-cm-wavelength Goldstone radar on 22 to 23 September 2000 revealed the presence of a narrowband spike that changed frequency in a manner indicative of an orbiting secondary (Fig. 1). Range-resolved data obtained on 23 September showed separations up to 2 km between the components and suggested that 2000 DP107 was a binary system (*7*). No additional antenna time was available at Goldstone, but a 10-day campaign of observations with the 13-cm-wavelength Arecibo radar on 30 September to 9 October confirmed the existence of a large orbiting secondary.

Most of the Arecibo observing time was devoted to obtaining range-Doppler images, in which radar echoes are resolved along two orthogonal dimensions, range and Doppler shift (*14*). A mosaic of radar images of 2000 DP107 obtained on eight successive days (Fig. 2) shows two well-separated components, with the primary showing the typical signature of a spheroidal object. Estimates of the component sizes can be determined from their range extents. Echo power exceeding three standard deviations of the noise is found in five to six consecutive range bins for the primary and two range bins for the secondary. Assuming that the true diameter of each object is about twice that of the radar-illuminated fraction, which experience with

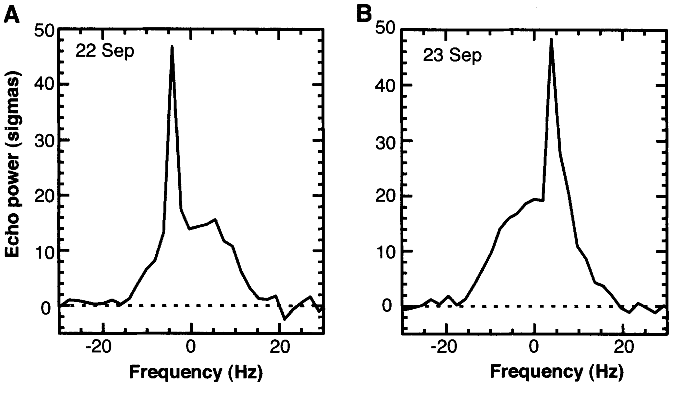

Fig. 1. Goldstone echoes resulting from a monochromatic transmission at 3.5-cm wavelength were spectrally analyzed at 2-Hz resolution and show a narrowband spike superposed on a broadband component. The wide-bandwidth echo is indicative of a rapidly rotating primary object, whereas the narrowband feature, which moves at a rate different from the rotation of the primary, represents power scattered from a smaller and/or slowly spinning secondary. The narrowband echo oscillates between negative and positive frequencies, representing the variations in Doppler shift of an object revolving about the system's center of mass. Data are from 22 September (**A**) and 23 September (**B**).

---

[1]California Institute of Technology, MC 150-21, Pasadena, CA 91125, USA. [2]National Astronomy and Ionosphere Center, Arecibo, Puerto Rico 00612. [3]Jet Propulsion Laboratory, 4800 Oak Grove Drive, Pasadena, CA 91109, USA. [4]Space Sciences Building, Cornell University, Ithaca, NY 14853, USA.

*To whom correspondence should be addressed. E-mail: margot@gps.caltech.edu